

Availability prediction method for EGNOS

Wei Zhi¹ · Zhipeng Wang¹ · Yanbo Zhu¹ · Rui Li¹

Received: 26 May 2016 / Accepted: 10 November 2016 / Published online: 25 November 2016
© Springer-Verlag Berlin Heidelberg 2016

Abstract Following the recent development of wide-area differential technology, satellite-based augmentation systems (SBASs) have been applied in many fields. However, the capability of monitoring stations used for generating error correction might degenerate with the aging of ground equipment over time, and the poor geometry between ranging and integrity monitoring stations (RIMS) and satellites could affect the reliability of navigation systems in supplying safety of life service. Therefore, it is necessary to predict SBAS availability so that users can choose a safe and efficient navigation system. Predictions of user difference range error indicator (UDREI) and grid ionospheric vertical error indicator (GIVEI) are the two difficulties in predicting SBAS availability. Considering the effect of geometry on UDREI, satellite geometric dilution of precision is defined to distinguish different geometries such that the relationship between the number of visible RIMS and UDREI in different geometries can be obtained. With regard to the effect of geometry on GIVEI, a weighted number of visible ionospheric pierce points (IPPs) is defined to describe the geometric IPP distribution such that the relationship between the number of visible IPPs and GIVEI in different geometries can be achieved. Finally, experiments are performed to evaluate the effectiveness of our proposed method. With the prediction algorithm, the prediction is consistent with actual performance over 75.17% of the entire European region. In particular, when focusing on central Europe, where the distribution of RIMS

is uniform, the level of consistency can reach 95–100%. It can be concluded that the prediction performance of the algorithm is encouraging and that this model may be considered a good contender for predicting SBAS availability.

Keywords European geostationary navigation overlay service · Grid ionospheric vertical error · User difference range error · Availability prediction algorithm · Satellite-based augmentation systems

Introduction

The ability to predict the availability of satellite navigation augmentation systems has become increasingly important. In the field of airborne-based augmentation systems, receiver autonomous integrity monitoring (RAIM) availability prediction has become an essential part of the system. This is because for a receiver to execute RAIM algorithm, two conditions must be met: a minimum number of satellites and adequate satellite geometry (Feng et al. 2006), which means RAIM does not work in some cases referred to as RAIM holes. Consequently, availability prediction must be conducted to exclude the risk of running into a RAIM hole. Currently, the USA, Australia, Germany, and China have developed mature RAIM availability prediction systems, and they demand that availability prediction be performed before using RAIM (Zhu et al. 2009). In the field of ground-based augmentation systems, the Federal Aviation Administration has clearly defined the requirements of availability prediction in the paper AC20-138B (FAA 2010). Research on ground-based augmentation system availability prediction has been undertaken (Wang et al. 2014), and the SLS-4000 Service Prediction Tool, developed by the Navigation Branch

✉ Zhipeng Wang
wangzhipeng@buaa.edu.cn

¹ National Key Laboratory of CNS/ATM, School of Electronic and Information Engineering, Beihang University, Beijing 100191, China

(ANG-C32), has been recommended for the Federal Aviation Administration as an acceptable method for meeting prediction requirements. In the field of satellite-based augmentation systems (SBASs), there is similar demand for availability prediction. Although research on this subject is limited, some relevant agencies, such as the European Satellite Services Provider (ESSP) and Iguassu Software Systems, have commenced research programs (Rovira-Garcia et al. 2015). We attempt to build a model to predict availability based on system architecture and the operational mechanism of SBASs.

SBASs are commonly composed of multiple ground-based monitoring stations, upload stations, and GEO satellites. With messages broadcast by GEO satellites, the SBAS supports wide-area or regional augmentation. The SBAS not only provides differential corrections, but it also ensures integrity, continuity, and availability. Currently, SBASs should meet the requirements of LPV-200. The European Geostationary Navigation Overlay Service (EGNOS) is the second most mature operational SBAS serving all the European countries. EGNOS consists of three segments: the space segment, ground segment, and user segment, as shown in Fig. 1. The space segment is composed of two geostationary satellites: AOR-E (PRN120) and SES-5 (PRN136) which took over the role of IOR-W (PRN126) on August 19, 2015. The main task of this segment is to maintain and implement communication between the RIMS and the master control center (MCC), as well as to transmit instructional information sent by the MCC to the users. The ground segment comprises 39 RIMS, 2 MCCs, and six navigation earth stations. The main task of this segment is to conduct comprehensive control and data processing for EGNOS. The user segment consists of EGNOS standard receivers, which need to be able to receive signals from EGNOS, GPS, and GLONASS simultaneously and interpret them compatibly. EGNOS has been used in applications such as aviation, marine, ground transportation (Gicquel et al. 2016).

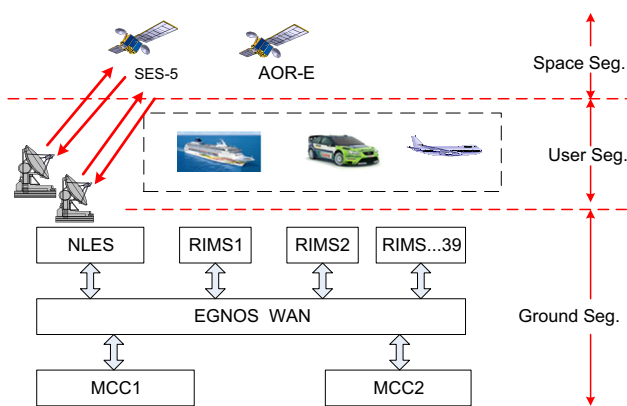


Fig. 1 Space segment, ground segment, and user segment of EGNOS

Inevitably, the capability of monitoring stations used for providing error corrections might degenerate over time, and poor geometry between the RIMS and satellites could affect the reliability of the navigation system in supplying safety of life (SOL) service. For example, a report has suggested that frequent road traffic accidents happened on Calle Hartzenbusch in Spain (Telegraph 2013). The lack of accurate corrections for GPS is believed to be an important factor. Coincidentally, accidents occurred in December 2014, when an Embraer aircraft prepared to land on a runway under the guidance of a satellite navigation system. Therefore, SBAS availability has become increasingly important. In summary, it is necessary to propose a method for predicting SBAS availability to avoid unnecessary losses.

Primary availability prediction algorithm

In this section, a primary availability prediction algorithm is proposed by the following three steps. First, through combing the calculation flow of SBAS availability, the difficulties of prediction algorithm are attributed to two real-time integrity parameters, user difference range error indicator (UDREI) and grid ionospheric vertical error indicator (GIVEI). Second, based on the calculation process of UDREI and GIVEI, the relationship between UDREI and the number of visible RIMS and the relationship between GIVEI and the number of visible ionospheric pierce points (IPPs) are analyzed statistically. Finally, experiments are performed to evaluate the effectiveness of the primary algorithm.

Calculation flow of SBAS availability

The Radio Technical Commission for Aeronautics specifies calculations for SBAS availability. In fact, SBAS availability depends on whether a user’s protection level (PL) is greater than the alarm limit. The vertical protection level (VPL) and horizontal protection level (HPL) can be calculated as follows (RTCA 2006):

$$HPL_{SBAS} = \begin{cases} K_{H,NPA} \cdot d_{major} & \text{for NPA} \\ K_{H,PA} \cdot d_{major} & \text{for PA} \end{cases} \quad (1)$$

$$VPL_{SBAS} = K_v \cdot d_U \quad (2)$$

where $K_{H,NPA}$, $K_{H,PA}$, K_v are the fractiles corresponding to the allocation of integrity risk under different approach modes. Furthermore,

$$d_{major} = \sqrt{\frac{d_{est}^2 + d_{north}^2}{2}} + \sqrt{\left(\frac{d_{est}^2 - d_{north}^2}{2}\right)^2 + d_{EN}^2} \quad (3)$$

$$\left. \begin{aligned} d_{\text{est}}^2 &= \sum_{i=1}^N S_{\text{east},i}^2 \sigma_i^2 & d_U^2 &= \sum_{i=1}^N S_{U,i}^2 \sigma_i^2 \\ d_{\text{north}}^2 &= \sum_{i=1}^N S_{\text{north},i}^2 \sigma_i^2 & d_{\text{EN}} &= \sum_{i=1}^N S_{\text{east},i} S_{\text{north},i} \sigma_i^2 \end{aligned} \right\} \quad (4)$$

where d_{major} is the error uncertainty along the semimajor axis of the error ellipse, d_{est}^2 is the variance of model distribution that overbounds the true error distribution in the east axis, d_{north}^2 is the variance of model distribution that overbounds the true error distribution in the north axis, d_{EN} is the covariance of model distribution in the east and north axes, d_U^2 is the variance of model distribution that overbounds the true error distribution in the vertical axis, $S_{\text{east},i}$ is the partial derivative of positional error in the east direction with respect to the pseudorange error on the i th satellite, $S_{\text{north},i}$ is the partial derivative of positional error in the north direction with respect to the pseudorange error on the i th satellite, and $S_{U,i}$ is the partial derivative of positional error in the vertical direction with respect to the pseudorange error on the i th satellite. The $S_{\text{east},i}$, $S_{\text{north},i}$, and $S_{U,i}$ are elements of the projection matrix S from the pseudorange domain to the position domain, which is defined as:

$$S = \begin{bmatrix} S_{\text{east},1} & S_{\text{east},2} & \cdots & S_{\text{east},N} \\ S_{\text{north},1} & S_{\text{north},2} & \cdots & S_{\text{north},N} \\ S_{U,1} & S_{U,2} & \cdots & S_{U,N} \\ S_{r,1} & S_{r,2} & \cdots & S_{r,N} \end{bmatrix} = (H^T W H)^{-1} H^T W \quad (5)$$

where H is an observation matrix corresponding to the geometry of the visible satellites, and W is a diagonal weight matrix corresponding to the variance of measurement noise.

The variance of measurement noise on the i th satellite is defined as:

$$\sigma_i^2 = \sigma_{i,\text{flt}}^2 + \sigma_{i,\text{UIRE}}^2 + \sigma_{i,\text{air}}^2 + \sigma_{i,\text{tropo}}^2 \quad (6)$$

where $\sigma_{i,\text{flt}}^2$ is the model variance for the residual error, $\sigma_{i,\text{UIRE}}^2$ is the model variance for the slant range ionospheric error, $\sigma_{i,\text{air}}^2$ is the model variance for the multipath receiver noise error, and $\sigma_{i,\text{tropo}}^2$ is the model variance for the tropospheric delay estimation error.

Analysis of the calculation process presented above indicates that the PL is determined by two factors. One is the geometry of the visible satellites, which could be predicted using a satellite almanac. The other is the standard deviation of the satellite pseudorange measurement, which consists of four parts: model variance for the residual error, model variance for the slant range ionospheric error, model variance for the multipath receiver noise error, and model variance for the tropospheric delay estimation error. The latter two are related to satellite elevation angles, which

means they also could be predicted using a satellite almanac. However, to predict the first two variances, we need two real-time integrity parameters broadcast by GEO satellites. One is UDREI, which is used to describe integrity related to the satellite clock/ephemeris error correction for each satellite. The other is GIVEI, which is used to describe integrity as related to the ionospheric error correction for each ionospheric grid point (IGP). Therefore, the focus here is on predicting UDREI and GIVEI through mathematical statistics.

Statistical treatment of UDREI

The user difference range error (UDRE) bounds the error of the computed ephemeris and clock corrections for each satellite with a probability of 0.999. The following important steps are used in the UDREI computation (Sardon et al. 1998).

1. Compute the residual error at the i th monitoring station, dR_i due to estimated range R_i and measured range R_{mi} as:

$$dR_i = R_{mi} - R_i \quad (7)$$

2. Estimate the mean \overline{dR} and standard deviation σ_R of the satellite’s ephemeris and clock error, respectively, for m monitoring stations as:

$$\overline{dR} = \frac{1}{m} \sum_{k=1}^m dR_k \quad (8)$$

$$\sigma_{dR} = \sqrt{\frac{1}{(m-1)} \sum_{k=1}^m (dR_k - \overline{dR})^2} \quad (9)$$

3. UDRE is a conservative tolerance error bound as:

$$\text{UDRE} = \overline{dR} + \kappa(\text{Pr}) \sigma_{dR} \quad (10)$$

where $\kappa(\text{Pr})$ is the statistical confidence factor given the confidence level Pr .

4. UDREI is obtained from UDRE using the conversion table specified by DO-229D.

Analysis of the above calculation process indicates that if a satellite has more visible RIMS, then it can get more pseudoranges, making the estimation of UDREI more accurate (Fang et al. 2013). Therefore, it is believed that a high correlation exists between UDREI and the number of visible RIMS, and practical measured data are processed to analyze their relationship. The processing procedure includes the following three steps. First, based on the positions of the RIMS and the satellite’s positions calculated from a satellite almanac, the number of visible RIMS for each satellite can be derived. Second, based on the satellite’s clock/ephemeris error correction information,

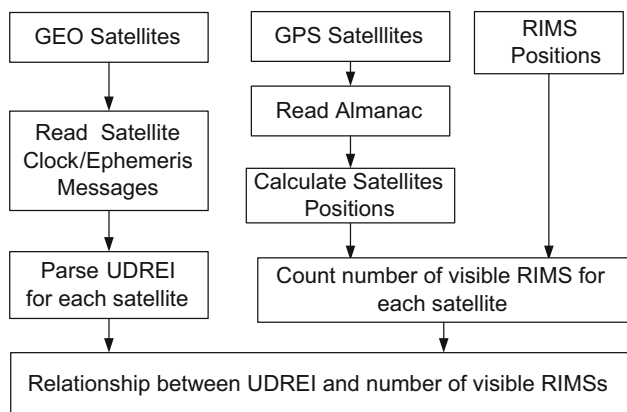


Fig. 2 Flowchart of the statistics and analysis of UDREI

broadcast by the GEO satellites, the UDREI value of each satellite can be parsed. Finally, according to the number of visible RIMS and the corresponding UDREI value for each satellite, the relationship between UDREI and the number of visible RIMS can be analyzed. Given this relationship, it would be possible to predict the UDREI of a satellite at any time, because the number of visible RIMS could be obtained easily from a satellite almanac. The processing flow is shown in Fig. 2.

Statistical treatment of GIVEI

There could be variations in the estimated delay at the IGP because of many error factors, e.g., modeling errors, mapping function errors, and measurement noise. These errors become translated from IPP locations to selected IGPs in the delay estimation process. Therefore, an error bound (grid ionospheric vertical error, GIVE) on such an error is also generated at each IGP. GIVE is the maximum error bound that an IGP can have. The error bound can be on either side of the estimated IGP delay value. The condition to GIVE estimation is that for every IGP there should be at least three surrounding squares, each with at least one IPP. This refers to the sufficiency of IPP density around an IGP. The following important steps are used in the GIVEI computation (Prasad and Sarma 2004):

1. Compute the residual error e_{IPP} due to the estimated user’s IPP delay \hat{I}_{IPP} and measured IPP delay I_{IPP} as:

$$e_{IPP}(t) = I_{IPP}(t) - \hat{I}_{IPP}(t) \tag{11}$$

2. Estimate the mean $|\bar{e}_{IPP}|$ and standard deviation σ_e of the user’s IPP vertical delays, respectively, for m epoch (i.e., time t_1 to t_m) measurements as:

$$|\bar{e}_{IPP}| = \frac{1}{m} \sum_{k=1}^m e_{IPP}(t_k) \tag{12}$$

$$\sigma_e = \sqrt{\frac{1}{(m-1)} \sum_{k=1}^m (e_{IPP}(t_k) - |\bar{e}_{IPP}|)^2} \tag{13}$$

3. Estimate the grid vertical absolute error bias \hat{e}_{IGP} at the surrounding four IGPs from the absolute value of the residual error at the i th user’s IPP, i.e., $|e_{IPP_i}(t)|$, for m epoch data using:

$$\hat{e}_{IGP} = \frac{\sum_{i=1}^n \left(\frac{1}{d_i}\right) \cdot |e_{IPP_i}(t)|}{\sum_{i=1}^n \frac{1}{d_i}} \tag{14}$$

where d_i is the distance from the i th user’s IPP to the selected IGP, and n is the number of IPPs adjacent to the selected IGP.

4. Generate a conservative tolerance error bound E_{IPP} for every valid user’s IPP in a surrounding square. E_{IPP} is derived from a two-sided statistical tolerance interval γ that contains a proportion p of a normally distributed population over a given sample size m as:

$$E_{IPP} = |\bar{e}_{IPP}| + g(\gamma; p; m)\sigma_e \tag{15}$$

where $|\bar{e}_{IPP}|$ is the absolute value of the mean error and $g(\gamma; p; m)$ is the statistical confidence factor. The confidence factor can be computed for given values of γ , p , and m . For $\gamma = 0.999$ (i.e., 99.9%), $p = 0.999$, and $m = 5$, $g(\gamma; p; m)$ is 23.54, and for $m = 30$, it is 5.43, i.e., it decreases with the number of data samples.

5. GIVE at the elected IGP is the sum of \hat{e}_{IGP} , maximum tolerance error bound $\max(E_{IPP})$, and an allowance for vertical ionospheric delay quantization q as:

$$GIVE = \max(E_{IPP}) + \hat{e}_{IGP} + q/2 \tag{16}$$

where $q = 0.0625$ m.

6. GIVEI is obtained from GIVE using the conversion table specified by DO-229D.

Although ionospheric delay is very dynamic, the residual error between the estimate value and the real value is relatively stable. Since GIVE is used to bound this residual error, the dynamic characteristic of GIVE is not obvious. Analysis of the above calculation process suggests it is possible to draw a law similar to that obeyed by UDREI, i.e., if the IGP has more visible IPPs, then it can get more ionospheric delay, making the estimation of GIVEI more accurate (Fang et al. 2013). Therefore, its value can be attributed to the number of visible IPPs. In fact, this view is reflected in many papers. Blanch (2002) points out that “integrity failures are more likely to happen when there are few IPP measurements.” Juan et al. (2002) believe that in regions well surrounded by IPP measurements, even in the

most adverse ionosphere conditions, delay estimate can be tightly bounded. Li et al. (2011) analyzed ionospheric delay estimation residuals over China and found in the central region of China where IPP measurements are sufficient, the confidence bound are small, at 0.1 m or less, while in the edge region where IPP measurements are sparse, confidence bound can reach more than 0.4 m. However, the above research only qualitatively revealed the relationship between the GIVE and IPP measurements; we will quantitatively analyze how the IPP measurements affect GIVE values.

Practical measured data are processed to analyze the relationship. The processing procedure includes the following four steps. First, based on the positions of the RIMS and the satellite’s positions calculated using a satellite almanac, the locations of the IPPs can be calculated. Second, having derived the locations of the IPPs and given the positions of the IGPs, the number of visible IPPs for each IGP can be obtained. Third, based on the ionospheric correction information, broadcast by the GEO satellites, the GIVEI value of each IGP can be parsed. Finally, according to the number of visible IPPs and the corresponding GIVEI value for each IGP, the relationship between GIVEI and the number of IPPs can be established. Given this relationship, it would be possible to predict the GIVEI of an IGP at any time, because the number of visible IPPs could be obtained easily from a satellite almanac. The processing flow is shown in Fig. 3.

Experiment and discussion

Currently, EGNOS has 39 operational RIMS and 287 IGPs, which are distributed in four vertical bands (band 3, band 4, band 5, and band 6) and one crosswise band (band 9). The positions of all the RIMS and IGP are known precisely, as shown in Fig. 4.

The broadcast data of EGNOS are available from EGNOS data collection stations at ENAC University in

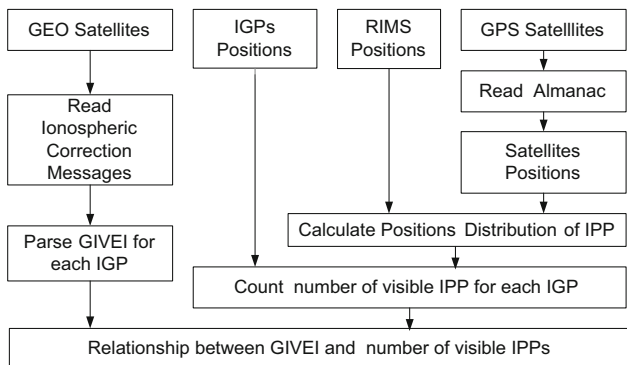


Fig. 3 Flowchart of the statistics and analysis of GIVEI

France. Here, 1 month of EGNOS data (December 1–30, 2014) were processed using the method presented above, and the result of the statistical treatment of UDREI is shown in Fig. 5.

It is evident from Fig. 5 that when the number of visible RIMS is small, the value of UDREI is 14, which means UDRE is not monitored. As the number of visible RIMS increases, UDREI decreases. When the number of visible RIMS reaches 32, the value of UDREI is 6.

The mean of UDREI for the same number of visible RIMS is calculated. To ensure the integrity of the system, the mean value is rounded up to be conservative; the results are shown in Table 1.

The result of the statistical treatment of GIVEI is shown in Fig. 6. It is obvious that when the number of visible IPPs is small, the value of GIVEI is 15, which means GIVE is not monitored. As the number of visible IPPs increases,

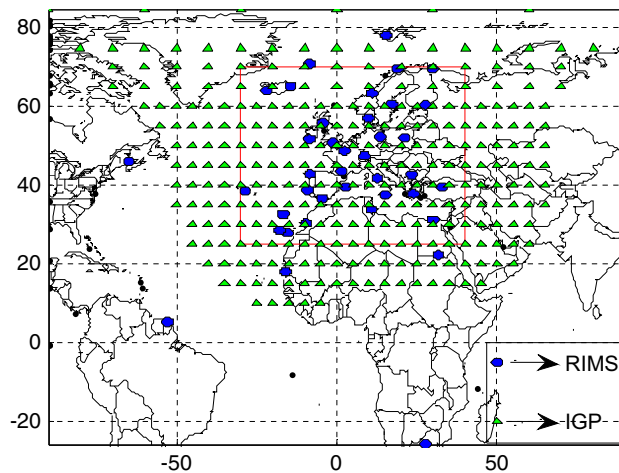


Fig. 4 Positions of RIMS and IGPs distributed in four vertical bands and one crosswise band of EGNOS

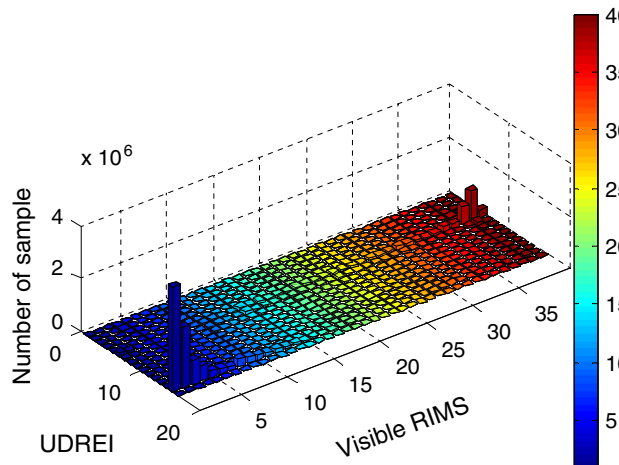


Fig. 5 UDREI sample distribution based on 1 month of EGNOS data

Table 1 Relationship between the number of visible RIMS and UDREI in EGNOS

Number of the visible RIMSs	UDREI value	Number of the visible RIMSs	UDREI value
0–7	14	14	8
8	13	15	8
9	12	16	8
10	11	17	8
11	11	18	8
12	10	19–31	7
13	9	32–39	6

Table 2 Relationship between the number of visible IPPs and GIVEI in EGNOS

Number of the visible IPPs	GIVEI value	Number of the visible IPPs	GIVEI value
0	15	6	11
1	15	7	11
2	14	8	10
3	14	9	10
4	13	10–14	9
5	12	≥15	8

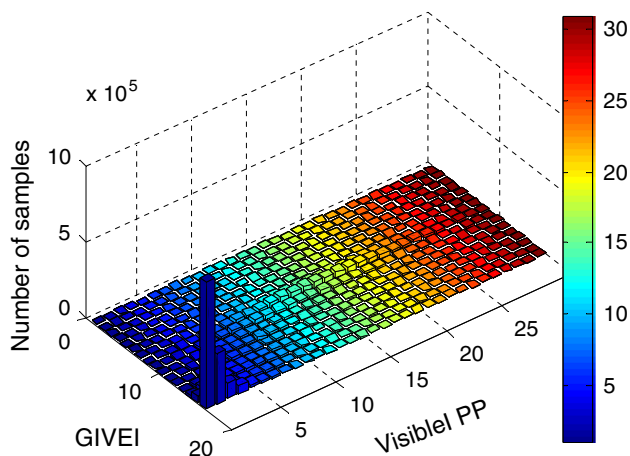


Fig. 6 GIVEI sample distribution based on 1 month of EGNOS data

GIVEI decreases. When the number of visible IPPs reaches 15, the value of GIVEI is 8.

The mean of GIVEI for the same number of visible IPPs is calculated. To ensure the integrity of the system, the mean value is rounded up to be conservative; the results are shown in Table 2.

Given the relationships shown in Tables 1 and 2, GIVEI and UDREI can be predicted, which means it should be possible to predict the standard deviation of the satellite pseudorange measurement. Then, by combining the standard deviation with the geometry of the satellites, the user’s VPL and HPL could be predicted. Furthermore, the availability of the SBAS could also be obtained. Based on the MATLAB Algorithm Availability Simulation Tool (MAAST), which is the SBAS simulation tool developed by GPSLAB of Stanford University (Jan et al. 2001), the availability prediction algorithm presented above is simulated. Prediction results for May 18, 2015, are shown in Figs. 7, 9 and 11.

To verify these prediction results, they were compared with maps (Figs. 8, 10 and 12) produced by ESSP, which is

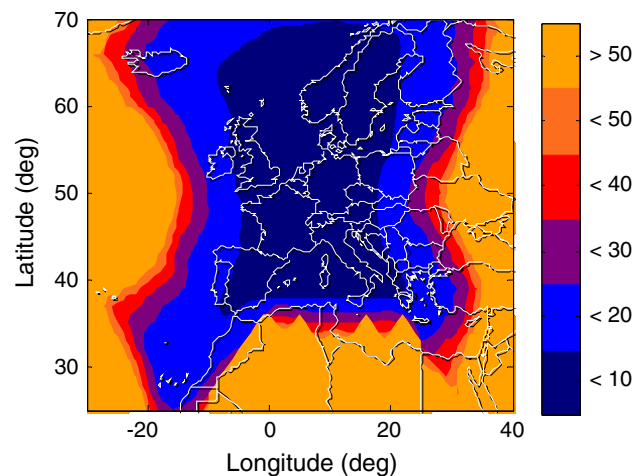


Fig. 7 Predicted HPL on May 18, 2015. Different colors represent different ranges of values as defined in color bar, e.g., the HPL of the red area is between 30 and 40 m

an authoritative institution monitoring the actual performance of EGNOS. It can be concluded that the prediction results are consistent with the actual performance in the central region, while a slight difference exists on the edge of the region.

ESSP provided quantitative values of actual availability so that further analysis could be undertaken. Figure 13 shows the difference between the actual and predicted availabilities. Statistical analysis demonstrates that the prediction is consistent with the actual performance over 72.28% of the region; it is smaller than the actual availability over 23.79% of the region and larger than the actual availability over 3.93% of the region.

These results indicate that the predicted availability conservatively reflects the actual availability. This means that as long as the predicted availability meets the operational requirements, the SBAS could be used safely with a probability of 96.07%.

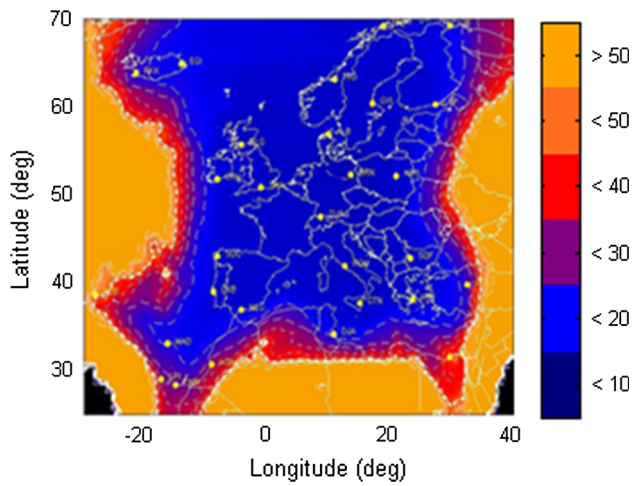


Fig. 8 Actual HPL on May 18, 2015. Different colors represent different ranges of values in meters as defined in color bar

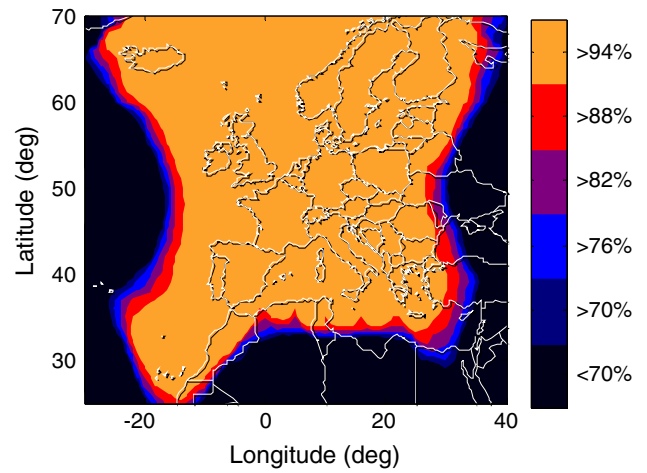


Fig. 11 Predicted availability on May 18, 2015. Different colors represent different ranges of values in percent as defined in color bar

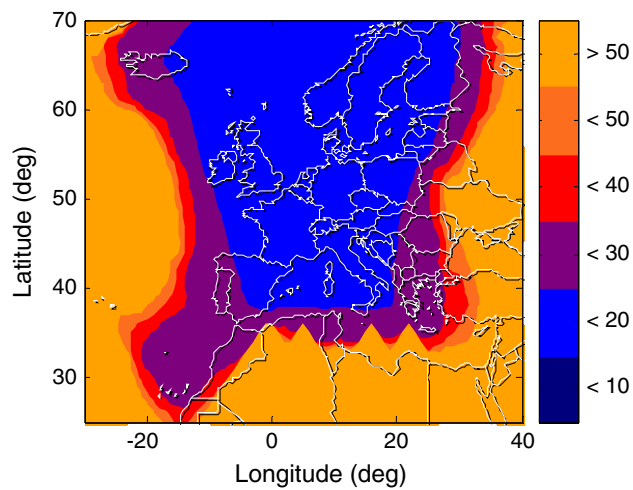


Fig. 9 Predicted VPL on May 18, 2015

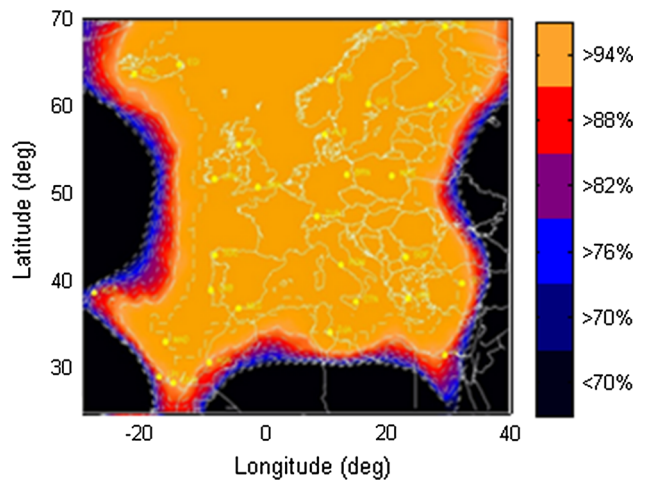


Fig. 12 Actual availability on May 18, 2015

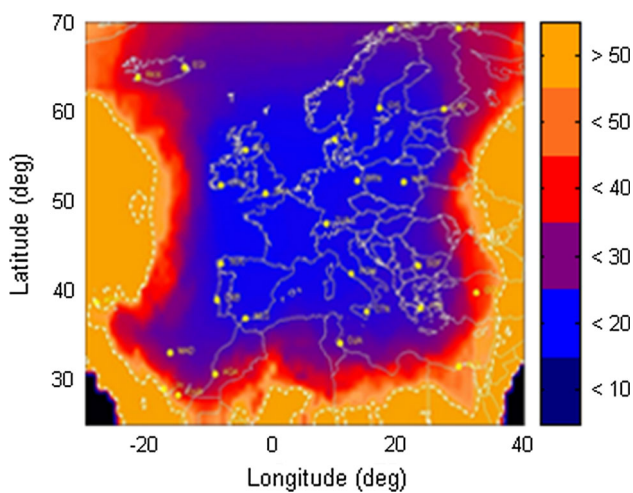


Fig. 10 Actual VPL on May 18, 2015

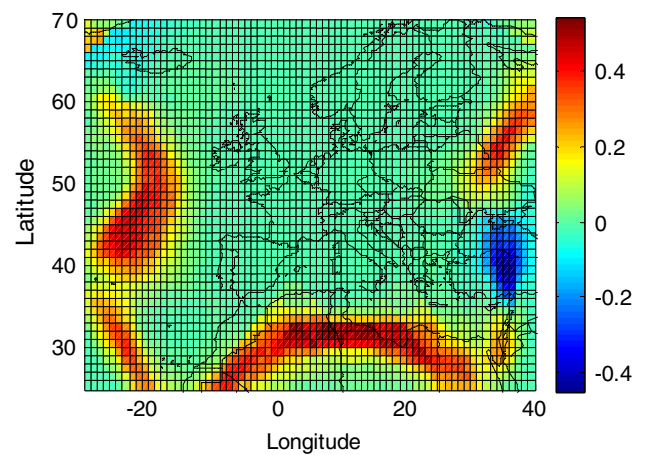


Fig. 13 Difference between the actual and predicted availabilities on May 18, 2015. Different colors represent different ranges of values as defined in color bar, e.g., in red area the prediction is 40% smaller than the reality

Improved availability prediction algorithm

In this section, an improved availability prediction algorithm is proposed which mainly contains three aspects. First, the necessity of data preprocessing is discussed and a new sampling strategy is defined to ensure sample independence. Second, considering the effect of geometry on UDREI, *S-GDOP* is defined to distinguish different geometries such that the relationship between the number of visible RIMS and UDREI for different geometries could be obtained. Third, with regard to the effect of geometry on GIVEI, a weighted number of visible IPPs is defined to describe the geometric distribution of the IPPs. Finally, experiments are performed to evaluate the effectiveness of the improved algorithm.

Independence of samples

As mentioned earlier, PL is the key indicator in predicting SBAS availability. PL overbounds the positioning error, which can be estimated using independent samples. Therefore, to improve the accuracy of the prediction, the independence of the samples must be guaranteed. However, in reality, the samples obtained are often not independent (Hauschild and Montenbruck 2016) because of the following two factors. First, the satellite ground trace repeats each day. Taking GPS as an example, every 23 h and 56 min, the relative position of the satellite and the user will repeat. This means that the multipath error related to the relative position has strong correlation in the adjacent time. It has been proven that variations in satellite orbits and ground conditions can cause the multipath error to become independent after 1 week (Shively et al. 2000). Thus, 1 week is skipped between samples in the improved algorithm. Second, when calculating the integrity parameters, the code measurements are smoothed with carrier phase measurements in a complementary filter with a 100-s time constant. Although this operation can effectively reduce the receiver noise and multipath error, it makes the adjacent pseudorange relevant. It is generally accepted that samples should be spaced two time constants apart to achieve acceptable independence (Luo et al. 2012). In summary, a new sampling strategy is obtained, which involves selecting 1 day each week and setting the sampling interval to 200 s for the selected day.

Under the new sampling strategy, the mean of UDREI for the same number of visible RIMS is calculated. To ensure the integrity of the system, the mean value is rounded up conservatively; the results are shown in Table 3, which upgrades Table 1 considering the effect of the independence of samples.

Then the mean of GIVEI for the same number of visible IPPs is calculated. The mean value is also rounded up

Table 3 Relationship between the number of visible RIMS and UDREI in EGNOS considering sample independence

Number of the visible RIMSs	UDREI value	Number of the visible RIMSs	UDREI value
0–7	14	14	8
8	13	15	8
9	12	16	8
10	11	17	8
11	10	18	8
12	10	19–31	7
13	9	32–39	6

Table 4 Relationship between the number of visible IPPs and GIVEI in EGNOS considering sample independence

Number of the visible IPPs	GIVEI value	Number of the visible IPPs	GIVEI value
0	15	6	11
1	15	7	11
2	14	8	10
3	13	9	10
4	12	10–18	9
5	12	≥19	8

conservatively to ensure the integrity of the system; the results are shown in Table 4, which upgrades Table 2 considering the effect of the independence of samples.

Given the relationships shown in Tables 3 and 4, GIVEI and UDREI can be predicted. Furthermore, the availability of the SBAS can be obtained. The prediction performance under the new sampling strategy is shown in Fig. 14, where it is clear that the difference between the actual and predicted availabilities transits gently in the edge region, in contrast to Fig. 13, which has noticeably sharper boundaries with the original sampling strategy. It means that the deviation is reduced in the edge region and that the performance of the prediction is improved under new sampling strategy.

Effect of geometry on UDREI

The UDREI prediction algorithm presented above only considers the number of RIMS, ignoring the effects of the geometry between the RIMS and satellites. In fact, the geometry has direct impact on the error distribution; thus, it also influences UDREI (Pandya et al. 2000). As analyzed earlier, UDREI has the following two characteristics: It describes the UDRE of a single satellite, and it is calculated using the pseudorange from a plurality of stations.

Before analyzing the impact of geometry, a variable must be defined that can describe such multi-station versus

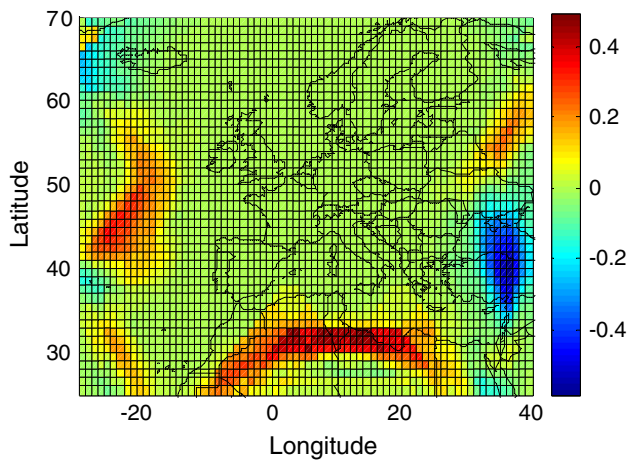


Fig. 14 Difference between the actual and predicted availabilities with the new sampling strategy

mono-satellite geometry, denoted S-GDOP, which can be defined as:

$$S - GDOP = \sqrt{G_{11} + G_{22} + G_{33} + G_{44}} \tag{17}$$

$$G = (H^T H)^{-1} \tag{18}$$

$$H = \begin{bmatrix} l_1 & m_1 & n_1 & 1 \\ l_2 & m_2 & n_2 & 1 \\ \vdots & \vdots & \vdots & \vdots \\ l_n & m_n & n_n & 1 \end{bmatrix} \tag{19}$$

This description refers to the definition of GDOP, except that the *i*th row of the observation matrix *H* here (i.e., [*l_i m_i n_i*]), is the line-of-site vector from the *i*th RIMS to the given satellite.

The correlation between UDREI and the number of visible RIMS as well as the correlation between UDREI and S-GDOP is analyzed (Fig. 15). It can be seen that when UDREI has a peak, the number of visible RIMS probably reaches a minimum and S-GDOP tends to be larger. Quantitative analysis indicates that UDREI displays strong correlation with the number of visible RIMS (Pearson Correlation = -0.72, *P* = 0) and weak correlation with S-GDOP (Pearson Correlation = 0.21, *P* = 4 × 10⁻³¹). When analyzing the effect of geometry on UDREI, two facts should be considered. The first is that the significance level of S-GDOP is 4 × 10⁻³¹, which means S-GDOP must be considered when predicting UDREI. The second is that the Pearson Correlation of S-GDOP is 0.21, which means S-GDOP is only a secondary factor; i.e., it is less important than the number of visible RIMS. Based on these facts, a new prediction algorithm is designed, where samples are grouped by S-GDOP, and then UDREI is predicted separately for each group using the traditional algorithm presented above. In this case, samples whose deviation of S-GDOP is within

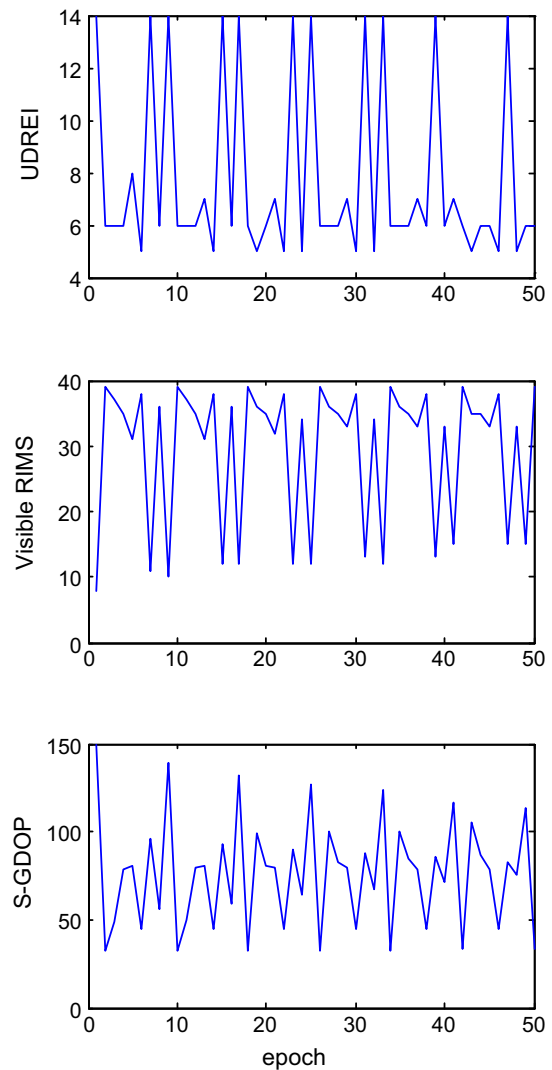


Fig. 15 Correlation analysis among UDREI, the number of visible RIMS and S-GDOP

100 were classified as a group because these samples are believed to have similar geometries.

Statistical analysis shows that when S-GDOP is small, the geometry between the RIMS and satellites is good. Consequently, the number of visible RIMS tends to be sufficient and the UDREI is small accordingly. As S-GDOP increases, the geometry deteriorates, making the number of visible RIMS decrease and UDREI increase simultaneously. To demonstrate this feature, the relationship between the number of visible RIMS and average of UDREI in different geometries characterized by S-GDOP is shown in Fig. 16. These curves generally display a downward trend showing the impact of the number of visible RIMS, and the different groups, characterized by S-GDOP, have slightly different curves, characterizing the impact of geometry. The tail of most curves is abnormal, because when S-GDOP is large, the geometry between the

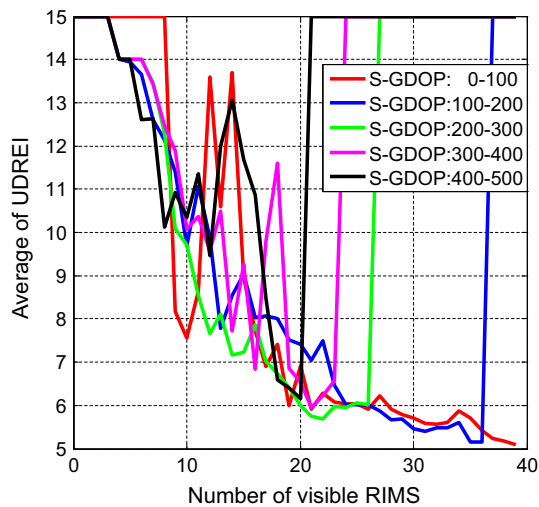


Fig. 16 Relationship between the number of visible RIMS and average of UDREI in different geometries characterized by S-GDOP

RIMS and satellites is poor. Hence, the maximum number of visible RIMS revealed in samples can no longer reach 40. In this situation, the predicted UDREI is set to 15 to indicate “unmonitored.”

To ensure the integrity of the system, the average of UDREI is rounded up conservatively; the results are shown in Fig. 17, which allows predicting UDREI with the given position of satellites and RIMS. The prediction is carried out through the following three steps: first, S-GDOP is computed as defined in (17); then, a specific color curve is selected according to the S-GDOP; finally, UDREI is predicted according to the number of visible RIMS with the selected curve.

Figure 18 shows consistency, i.e., the percentage of the area where the prediction is consistent with the reality, as a function of number of groups. The consistency between the prediction and reality is chosen as an indicator for evaluating the performance of the algorithm for different numbers of groups. For a larger number of groups, geometry is considered more adequately because the deviation of S-GDOP in each group becomes less. However, it does increase the complexity of the algorithm because more prediction curves need to be analyzed. In the meanwhile, an increase in the number of groups means a reduction in the number of samples within a single group, which could diminish the credibility of the statistical results. The figure shows that when the number of groups is small, an increase in that number improves the consistency significantly. When the number reaches three, the consistency tends to vary slightly with a further increase in the number of groups. When the number of groups reaches five, optimum consistency is achieved, which means the geometry has been considered adequately. If the number of groups is increased further, the consistency declines because

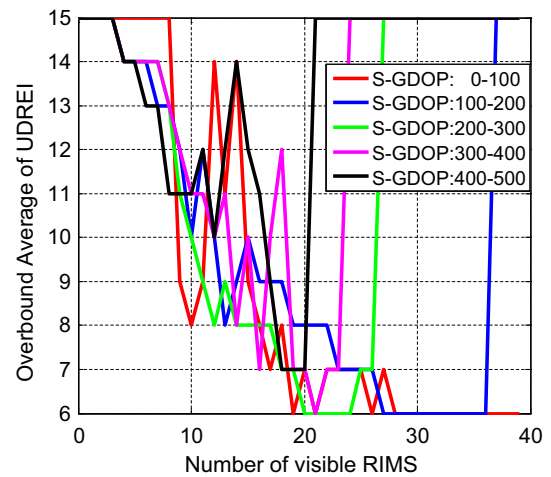


Fig. 17 Relationship between the number of visible RIMS and overbound average of UDREI in different geometries characterized by S-GDOP

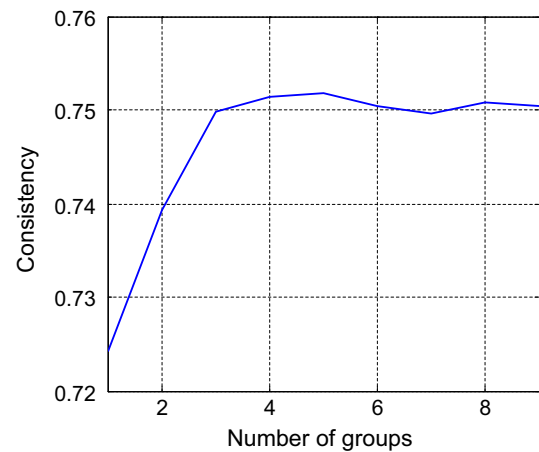


Fig. 18 Effect of the number of groups on consistency, i.e., the percentage of the area where the prediction is consistent with the reality

overfitting magnifies the influence of accidental errors (Hawkins 2004). In our research, the number of groups is set to five, which is based on the result of the analyses shown in the figure.

Effect of geometry on GIVEI

As discussed above, GIVEI has been modeled as a function of the number of visible IPPs, denoted N . This count can capture approximately the law of change for GIVEI. However, it omits the details of the geometric distribution of the IPPs. It is obvious that an IPP closer to the IGP contributes more when calculating GIVEI than one further away. According to the Triangular Interpolation (TRIN) model (Mannucci et al. 1993) adopted by EGNOS (Trilles et al. 2015), when interpolating the ionospheric delay of the

IGP, inverse-distance weighting is believed to roughly weigh each IPP’s contribution to the generation of GIVEI. Thus, a weighted number of visible IPPs, denoted N_{weighted} , is defined as:

$$N_{\text{weighted}} = \sum_i \frac{C}{d_i} \tag{20}$$

where the summation goes over the visible IPPs, d_i is the distance between the i th IPP and the IGP, and C is the constant distance between the IGP and the selected IPP whose weight is 1.

The relationship between the weighted number of visible IPPs and GIVEI is shown in Fig. 19. The top panel reveals the relationship between this number and the average of GIVEI. To ensure the integrity of the system, the average of GIVEI is rounded up conservatively; the results are shown in the bottom panel. The curve is believed to better predict GIVEI than Table 2, because it considers the details of the geometric distribution of the IPPs.

Performance of improved algorithm

With the improved algorithm, the predicted PL and availability are obtained. Quantitative analysis of the improved algorithm is shown in Fig. 20. The statistical analysis of the difference demonstrates that the prediction is consistent with the actual performance over 75.17% of the region; it is

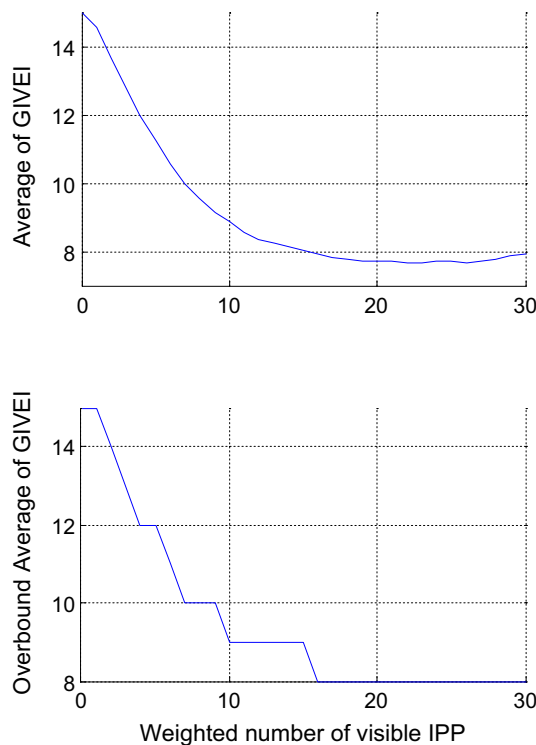


Fig. 19 Relationship between the weighted number of visible IPPs and GIVEI in EGNOS

smaller than the actual availability over 22.14% of the region, and it is larger than the actual availability over 2.69% of the region. In particular, when focusing on Region I, shown by the red box in the figure (longitude -10° to 16° , latitude 37° – 58°), the consistency can be up to 100%. This can be explained by the geometric distribution of RIMS. Apparently, the RIMS distribution in Region I is uniform, whereas in the edge regions, where the performance of the prediction algorithm is poor, the RIMS distribution is deficient.

The core of the prediction model is to obtain the number of visible RIMS and the number of visible IPPs. The height of the ionospheric spherical shell is so low in comparison with the height of the satellite that the geometric distribution of the IPPs can be approximately characterized by the geometric distribution of RIMS. Therefore, it is reasonable that the performance of the prediction algorithm is highly correlated with the geometric distribution of RIMS. To analyze this phenomenon quantitatively, two indicators that describe the geometric distribution of RIMS are defined. The first is the number of RIMS per unit area, denoted N_{wrs} , which is defined as:

$$N_{\text{wrs}} = \frac{N_{\text{area}}}{S_0} = \frac{N_{\text{area}}}{S_{\text{area}}/S_{\text{total}}} \tag{21}$$

where N_{area} is the number of RIMS in the given area, S_{area} is the proportion of the given area, S_{total} is the proportion of Europe, and S_0 is the normalized proportion of the given area.

The second indicator is the average distance of the total station pairs, which is an assembly consisting of any two stations, in the given area, and denoted D_{pairs} , which is defined as:

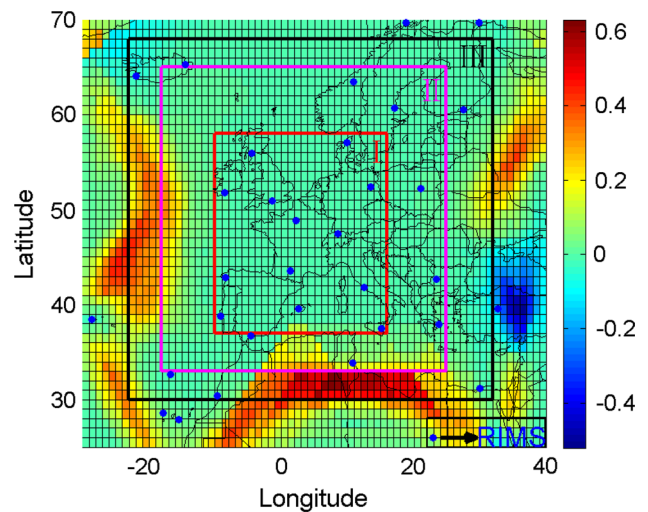


Fig. 20 Difference between the actual and predicted availabilities with the improved algorithm. Region I is shown by the red box (longitude -10° to 16° , latitude 37° – 58°); Region II is shown by the purple box (longitude -18° to 25° , latitude 33° – 65°); Region III is shown by the black box (longitude -23° to 32° , latitude 30° – 68°)

Table 5 Performance of the improved algorithm in different regions

Area	Region I	Region II	Region III	Total region
Consistency	100%	95.16%	85.64%	75.17%
N_{wrs}	75.00	45.78	39.19	32.00
D_{pairs} (10^6 m)	1.29	1.62	2.04	2.36

$$D_{\text{pairs}} = \frac{\sum_{i=1}^N d_i}{N} \quad (22)$$

where d_i is the distance of the i th station pair, and N is the total number of possible station pairs.

The performance of the improved algorithm in different regions is shown in Table 5. It is evident that if N_{wrs} is large and D_{pairs} is small, the geometric distribution of RIMS tends to be good, making the prediction more precise (Yun 2015).

Conclusions

The aim of this research was to investigate a simplified method for predicting SBAS availability, given the intense computation and poor timeliness of the traditional algorithms specified in DO-229D. Our contribution is as follows. First, the relationship between UDREI and number of visible RIMS and between GIVEI and number of visible IPPs was established through statistical analysis of EGNOS data. Second, considering the effect of geometry, the relationship was optimized for application with different geometries. Given the relationship, a simplified calculation of PL was demonstrated.

Finally, experiments were performed to evaluate the effectiveness of the proposed method. Using the proposed method, in Region II, where N_{wrs} is 45.78 and D_{pairs} is 1.62×10^6 , the consistency between the predicted and actual availabilities reached 95.16%. With improvement of the geometric distribution of RIMS in the given area, the performance of the prediction becomes even better. In particular, when the application range of the prediction algorithm is limited to Region I, where N_{wrs} is 75.00 and D_{pairs} is 1.29×10^6 , indicating a uniform distribution of RIMS, the consistency reached 100%. Moreover, the prediction method proposed in this work could be extended easily to other SBAS systems. This research may provide BeiDou satellite-based augmentation systems with theoretical and technical guidance, particularly in the layout of its ground stations and design of ionospheric grid.

It must be acknowledged that the performance of the prediction algorithm over the entire European region is not that satisfactory (75.17%). The lack of RIMS at the edges of the region is the main reason for this problem, i.e., the scarcity of a priori information results in inaccuracy of the prediction algorithm. In terms of the presented

methodology, we only considered the mean of the integrity parameters to make the predictions, ignoring the impact of variance, which might cause a difference between the prediction and the actual performance. Quantitative analysis of the effect of variance should be addressed with respect to the integrity of the prediction, which was not the focus here. Furthermore, the inverse-distance weighting regarding the prediction of GIVEI may be optimized by a Kalman Filter to adapt to different SBASs. Then PL at each epoch, which is not public, needs to be provided. Finally, we set the elevation mask angle to 5° to determine whether a satellite was visible, which might be impractical. This will be considered in future work as long as access to real geographic information on the EGNOS RIMS is available. However, it might be considered worth sacrificing some degree of accuracy in exchange for improved predictability.

Acknowledgements The authors would like to give thanks to many people for their advice and interest. Christophe Macabiau from École Nationale de l'Aviation Civile provided rounded guidance on the technical details of the paper. Norbert Suard from Centre National d'Études Spatiales patiently provided all the positional information regarding the ranging and integrity monitoring stations of Geostationary Navigation Overlay Service (EGNOS). Ridha Chaggara from European Satellite Services Provider offered the actual EGNOS availability. Without the kind assistance of these people, this work could not have been conducted. This work was undertaken with financial support from the National Natural Science Foundation of China (Grant No. 61501010), Beijing Municipal Natural Science Foundation (Grant No. 4154078), and Aeronautics Science Foundation (Grant No. 2015ZC51035).

References

- Blanch J (2002) An ionosphere estimation algorithm for WAAS based on Kriging. In: Proceedings of ION GPS 2002, Institute of Navigation, Portland, OR, September 24–27, pp 816–823
- FAA A (2010) AC 20-138B-airworthiness approval of positioning and navigation systems. http://www.faa.gov/documentLibrary/media/Advisory_Circular/AC%2020-138B.pdf
- Fang JS, Zhu YB, Wang ZP (2013) Key parameters processing and analysis for EGNOS integrity. *J Civ Aviat Univ China* 31(1):13–17
- Feng S, Ochieng WY, Walsh D, Ioannides R (2006) A highly accurate and computationally efficient method for predicting RAIM holes. *J Navig* 59(01):105–117
- Gicquel JA, Arnaud D, Gouni P (2016) EGNOS V3: engineering the future of GPS and Galileo augmentation over Europe. *Complex systems design and management*. Springer, Berlin, p 289
- Hauschild A, Montenbruck O (2016) A study on the dependency of GNSS pseudorange biases on correlator spacing. *GPS Solut* 20(2):159–171
- Hawkins DM (2004) The problem of overfitting. *J Chem Inf Comput Sci* 44(1):1–12
- Jan SS, Chan W, Walter T, Enge P (2001) Matlab simulation toolset for SBAS availability analysis. In: Proceedings of ION GPS 2001, Institute of Navigation, Salt Lake City, UT, September 2001, pp 2366–2375
- Juan B, Todd W, Per E (2002) Ionospheric threat model methodology for WAAS. *Navigation* 49(2):103–107

- Li X, Zhu Y, Xue R (2011) Ionospheric delay correction and integrity monitoring based on Kriging in GRIMS. *Energy Proc* 13:659–667
- Luo Y, Babu R, Wu WQ, He XF (2012) Double-filter model with modified Kalman filter for baseband signal pre-processing with application to ultra-tight GPS/INS integration. *GPS Solut* 16(4):463–476
- Mannucci AJ, Wilson BD, Edwards CD (1993) A new method for monitoring the earth's ionospheric total electron content using the GPS global network. In: *Proceedings of ION GPS 1993*, Institute of Navigation, Salt Lake City, UT, September 1993, pp 1323–1332
- Pandya N, Wu JS, Grewal M (2000) Dependence of GEO UDRE on ground station geometries. In: *Proceedings of ION NTM 2000*, Institute of Navigation, Anaheim, CA, January 2000, pp 80–90
- Prasad N, Sarma AD (2004) Ionospheric time delay estimation using IDW grid model for GAGAN. *J Indian Geophys Union* 8(4):319–327
- Rovira-Garcia A, Juan JM, Sanz J, González-Casado G, Ibáñez D (2015) Accuracy of ionospheric models used in GNSS and SBAS: methodology and analysis. *J Geodesy* 90(3):229–240
- RTCA DO229D (2006) Minimum operational performance standards for global positioning system or wide area augmentation system airborne equipment, Tech Rep DO229D, RTCA
- Sardon E, La Fuente JAD, Zarraco N, Nieto J, Cosmen J (1998) Udre computation: a key issue for space based augmentation system performance. In: *Proceedings of ION GPS 1998*, Institute of Navigation, Nashville, TN, September 15–18, pp 2091–2100
- Shively CA, Braff R (2000) An overbound concept for pseudorange error from the LAAS ground facility. In: *Proceedings of ION AM 2000*, Institute of Navigation, San Diego, CA, June 26–28, pp 661–671
- Telegraph (2013) Five drivers follow satnav down the stairs in Spanish town. <http://www.telegraph.co.uk/news/worldnews/europe/spain/10094276/Five-drivers-follow-satnav-down-the-stairs-in-Spanish-town.html>
- Trilles S, Authié T, Renazé C, Raoul O (2015) Robust EGNOS availability performances under severe ionospheric conditions. In: *Proceedings of ION GNSS + 2015*, Institute of Navigation, Tampa, Florida, September 14–18, pp 1783–1789
- Wang ZP, Macabiau C, Zhang J, Escher AC (2014) Prediction and analysis of GBAS integrity monitoring availability at LinZhi airport. *GPS Solut* 18(1):27–40
- Yun Y (2015) Influence of reference station distribution on the Korean SBAS performance. In: *Proceedings of ION PNT 2015*, Institute of Navigation, Hawaii, April 20–23, pp 964–969
- Zhu Y, Zhang M, Zhang J (2009) Research on weighted algorithm to predict RAIM availability. *J Telem Track Command* 01:1–6



Wei Zhi received his B.S. in Electronic and Information Engineering from school of Electronic Information Engineering, Beihang University in 2014. He currently is a graduate student in the National Key Laboratory of CNS/ATM at Beihang University. His main research interest is Satellite-Based Augmentation System.



Zhipeng Wang received B.S. in communication engineering from the School of Electronic Information and Engineering, Northwestern Polytechnical University (NWPU) in 2006, and received Ph.D. in Traffic Information Engineering from School of Electronic Information Engineering, Beihang University in 2013. He currently is a lecturer in School of Electronic Information and Engineering, Beihang University. His research focuses on the combination algorithms of Ground-Based Augmentation System (GBAS) and Satellite-Based Augmentation System (SBAS), also Advanced Receiver Autonomous Integrity Monitoring (ARAIM).



Yanbo Zhu received B.S. and M.S. degrees from School of Electronic Information Engineering, Beihang University in 1992 and 1993, respectively. He is currently a Ph.D. candidate in School of Electronic Information Engineering, Beihang University and chief engineer of CNS/ATM labs, CAAC. His major research interests are air traffic management, aeronautical telecommunication network, satellite navigation and automatic dependent surveillance.



Rui Li received his Ph.D. degree from Beihang University in 2006. He is now a senior engineer in the school of Electronics and Information Engineering at Beihang University. His main interests cover RNP and GNSS augmentation technologies in SBAS, GBAS, and ABAS.